11th Asia-Pacific Conference on Combustion,

The University of Sydney, NSW Australia
10th -14th December 2017.

Hypergolic Ignition Induced by Binary Collision of TMEDA and WFNA Droplets: Non-monotonic Effects of Impact Parameter

Dawei Zhang, Peng Zhang*

Department of Mechanical Engineering

The Hong Kong Polytechnic University, Kowloon, Hong Kong

Abstract

Ignition delay of hypergolic bipropellants of TMEDA and WFNA by their binary droplet collision has been experimentally studied, with the particular emphasis on the effects of impact parameter, *B*, which measures the deviation of the collision from the trajectory of head-on situation. The experimental results reveal a non-monotonic effect of the impact parameter. For *B* slightly larger than 0, the intrinsic deformation and internal flow pattern promote the mixing between the colliding droplets and hence reduce the ignition delay. If *B* increases to so that off-center separation happens, the hypergolic ignition would be prolonged owing to the less mass transfer.

1 Introduction

Being widely adopted for the space propulsion applications, the hypergolic bipropellant has been of great interests in the past decades[1-3]. Unlike the ignition of a homogenous mixture of non-hypergolic reactants, the auto-ignition of the hypergolic bipropellants essentially relies on the mixing process between the liquid fuel and oxidizer preceding the eventual gas-phase ignition[3].

Many experimental efforts have been made in order to quantify the influence of the liquid-phase mixing process on the hypergolic ignition[4-7]. In spite of the worthy knowledge obtained from these previous studies, the liquid-phase mixing effect remains quantitatively uncertain because of the existence of the "wall effect" from their experimental facilities.

Recently, an experimental apparatus with capability of eliminating all the "wall effect" was designed and established by the authors, through which the hypergolic ignition of N,N,N',N'–tetramethylethylenediamine (referred to as TMEDA hereinafter) and white fuming nitric acid (referred to as WFNA hereinafter) was investigated by the binary collision of 'freely' moving droplets[8]. The focus of the study was mainly placed on the head-on collisions at variable collision Weber numbers(*We*s) and size ratios(*Δ*s). Hypergolic ignition delay of the bipropellants was thereby interpreted by using the previous knowledge of the mixing and interaction effects in non-reactive head-on droplet collisions[9-10]. Nevertheless, it is noted that the axisymmetric head-on collision is a rare event in the real situation and the almost sure events are off-center collisions.

To quantify off-center collisions, a dimensionless impact parameter, *B*, is defined as the ratio of the projection of the distance of two droplet centers to the direction of their relative velocity, χ, to the sum of the two droplet radii, $(D_S + D_L)/2$, and more specially $B = 2\chi/(D_S + D_L)$ [11]. The head-on collision corresponds to $B = 0$, off-center collisions to $0 < B < 1$, and a grazing collision to $B = 1$.

It has been found that *B* affects not only the outcomes of the binary collisions but also the mixing during the collision process [12]. Specifically, it has been numerically found that a non-monotonic variation of the mixing rate with *B* would exhibits at various collision *We*s[13-14]. Whether the hypergolic ignition induced by the off-center collision of TMEDA and WFNA would be in line with this trend is the question that merits studies.

Motivated by the foregoing concerns, the present study aims mainly to experimentally study the hypergolic ignition characteristics of bipropellants of WFNA and TMEDA by their off-center droplet collisions with intricate mixing patterns and fluid physics. We therefore present the study as follows. The experimental apparatus and the measurement methods are expatiated in Section 2. The results for four representative cases are presented in Section 3 to illustrate the hypergolic ignition processes. Dependence of ignition delay on the impact parameter is presented in Section 4, followed by concluding remarks in Section 5.

2 Experimental Specifications

The experimental specifications have already been expatiated in our previous paper [8] and therefore only a brief description is given herein. Droplets of WFNA and TMEDA were generated by two unlike and independently controlled droplet generators, each of which is fastened on a XYZ microscope stage through which the generator could be adjusted precisely in both the dispensing positions and angles. As with intensive corrosivity, the WFNA droplet was generated by using an in-house needle-shape nozzle, which was manufactured with the highly anti-corrosion material of Teflon (Polytetrafluoroethylene). With the carefully arranged connecting pipe and driving pressurized ultra-pure nitrogen gas, the WFNA droplet size was able to be fixed at 1.45mm at constant generation frequency. The electromagnetic micro-valve made by Fritz Gyger AG was employed to generate TMEDA droplets, whose sizes vary from 0.2mm to 1.5 mm. Temporally and spatially stable collisions between the TMEDA and WFNA droplets were achieved by precisely adjusting the tunable droplet generation time and the position of XYZ stage.

A high speed camera V711 from Phatom was adopted to record shadowgraph images of the collision and ignition processes with a fixed sampling rate of 5000fps and a fixed shutter time of 5μs. A MATLAB program was developed to help analyze the images in determining the diameters, the impact velocities and the impact parameter, *B*. The measurement of *B*, as shown in

Corresponding author.

E-mail address: pengzhang.zhang@polyu.edu.hk

Fig.1, relies on the measureent of two velocity vectors at an appropriate temporal interval. The measurement error for droplet diameter and impact parameter are less than 7%, and the uncertainty of measured droplet velocity, which is determined by averaging the displacement of the droplet center during five successive images (i.e. 1.0ms), is about 3%-8%.

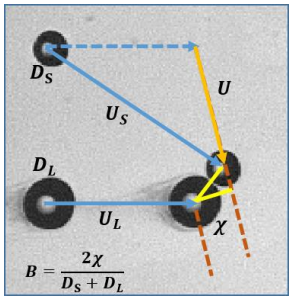

Figure 1. The procedure of the calculation of impact parameter *B* in experiment for hypergolic ignition by binary off-center collision of TMEDA and WFNA droplets.

A grayscale analysis of the shadowgraph images as proposed in our previous study also is applied to precisely determine the ignition delay time with an uncertainty of less than 0.2 ms. Such an analysis is based on that large difference of grayscale levels (0-256) can emerge in the shadowgraph images, where the darkest areas (levels are lower than 5) are occupied by droplets and their vapors; the brightest areas (levels are higher than 250), by luminous ignition kernels and flames. A photodetector and an infrared detector has been employed in our previous study to verify the reliability and accuracy of the grayscale analysis.

3 Phenomenological Description

3.1 Hypergolic Ignition

In order to characterize the off-center (impact parameter) effect in the present study, four representative collisions with various *B*s of 0, 0.3, 0.6 and 0.9, but with fixed *We* = 60.9, Δ = 1.6 and $Oh = 2.5\times10^{-3}$ are presented, in which the Weber number, *We*, measurs the relative importance of droplet inertia compared with its surface tension, size ratio, Δ, is defined by the ratio of the diameter of the bigger droplet to that of the smaller one, impact parameter, *B*, is as defined above and Ohnesorge number, *Oh*, is adopted to measure the importance of viscous force relative to surface tension,

Figure 2 shows in the sequence of both the physical time and dimensionless time, $T = t/t_{\mathrm{osc}}$ where $t_{\mathrm{osc}} = \sqrt{\rho_o R_o^3/\sigma_o}$ is approximately the natural oscillation time of the WFNA droplet, the entire collision and ignition processes for the four representative cases. For a clear description of the entire ignition process, multiple length scales were adopted as indicated on the images. The initial moment, *t* = 0, is defined when the two droplets were just about to collide.

As shown in Fig.2, in the initial stage from 0ms to about 3ms, the interaction between the colliding TMEDA and WFNA droplets for all the four cases are similar to those non-reactive collisions.[12] Reflexive deformation dominates in the collision of *B* = 0 and *B* = 0.3, while the two droplets tend to stretch away from each other at *B* = 0.6 and *B* = 0.9. Since the merged droplet was heated up by the exothermic liquid-phase reaction, opaque vapors and gaseous species were generated and started to expand outwardly at around 3.6ms for all the four collisions. The opaque gas-phase matters continued growing so that the surface of the merged droplet at *B* = 0 and 0.3 and the separated droplets with the satellite droplets at *B* = 0.6 and 0.9 are blurred or even concealed inside the dark vapor and gaseous products, as seen at 11.4ms. The flame, indicated by the luminous overexposure area on the shadowgraphs, can be observed at the moments of 31ms, 25ms and 33.0ms for collisions *B* = 0, *B* = 0.3 and *B* = 0.6 respectively. While no bright flame occurs throughout the whole period for collision *B* = 0.9, so it should be regarded as non-ignitable. Non-combustible products or unburned extra reactants could be observed along with or after the luminous flame, as indicated on the images.

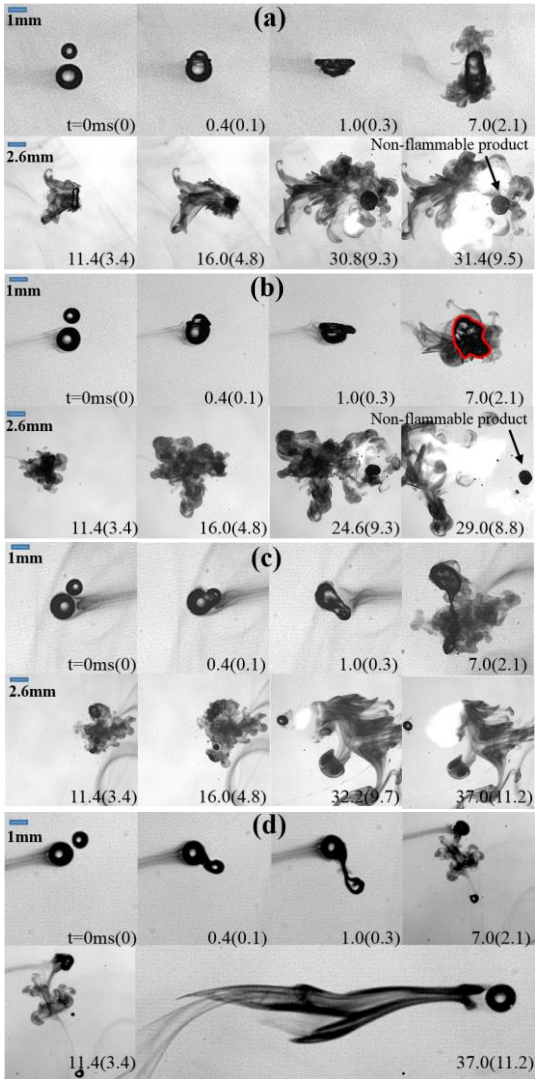

Figure 2. Shadowgraph images of the hypergolic ignition at selected times for a representative case with *We*=60.9 and Δ=1.6 and (a) *B* = 0; (b) *B* = 0.3; (c) *B* = 0.6; (b) *B* = 0.9.

3.2 Impact Parameter Effects on Mixing, Evaporation and Ignition

To systemically describe and analyze the evaporation and condensed phase chemical reaction processes, we quantified the pixel-area occupied by the opaque matters in the shadowgraph images by a normalized parameter of r_d. The time-dependent ratio of r_d is defined by [8]

$$r_d = N_d(t|G < G_{low})/N \quad (1)$$

where $N_d(t|G < G_{low})$ is the total number of pixels having the grayscale levels, G, lower than G_{low}; *N* is the total number of pixels in the image.

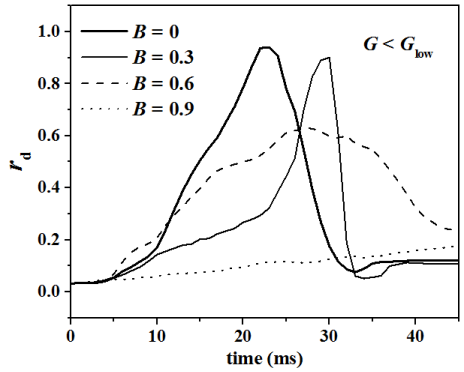

Figure 3. Grayscale level analysis of r_d for the representative cases shown in Figure 2.

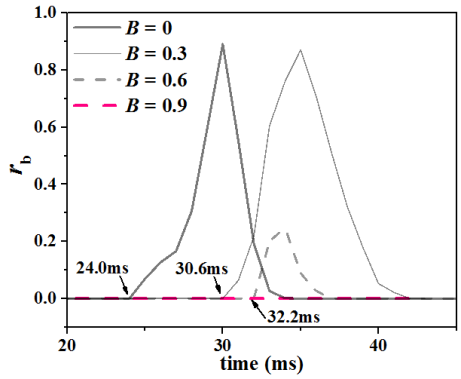

Figure 4. Grayscale level analysis of r_b for the representative cases shown in Figure 2.

As shown in Fig 3, r_d remains the lowest level at the beginning for almost the same time duration for all the four collisions and begins to rise up afterwards. In the following growth period of the opaque matters, the peak values of the occupying area at B = 0.6 and B = 0.9 are much smaller than those for B = 0.0 and B = 0.3. The underlying reason is that, since the stretching separation happens at B = 0.6 and B = 0.9, it diminishes the amount and time period of mass transfer between the droplets and hence impairs the evaporation and condensed phase chemical reactions.

Another interesting phenomenon is that the starting instant of the rapid evaporation stage comes about 10ms earlier at B = 0.3 than the head-on collision. The difference in the duration of the rapid evaporation stage is owing to the different mixing efficiencies for the two merging collisions. When the two droplets collide with non-zero impact parameters, both reflexive interaction and stretching will effect and a four-lobe-shape drop would therefore always be formed, as shown in the shadowgraph at 7.0ms for the collision at B = 0.3. The droplet internal under the competing effects would be more complicated than it does in the head-on collision under symmetric reflexive interaction. The intricate internal flow will thereby enhance the mixing and expedite the evaporation.

Based on the observation and analysis above, we found that the impact parameter would influence the mixing between the two droplets in two competing ways. At relatively small Bs, for example, B = 0.3, the reflexive interaction is dominant and it strengthens the mixing by the "jet-like" internal flow patterns [17]. While the mixing enhancement will be weakened due to the reduced time for mass transfer if stretching separation happens at higher Bs.

Affected by the mixing of the fuel and oxidizer and the accompanying evaporation, the hypergolic ignition delay is therefore related to the impact parameter effect. Another normalized parameter, $r_{b,}$ whish is silimar to r_d but with a high threshold of grayscale level of G_{high}, representing the development of the luminous flame was employed to quantitatively identify the ignition delay. As shown in Fig. 4, the ignition delay times for the three ignitable representative collisions B = 0, B = 0.3 and B = 0.6 are 30.6ms, 24.0ms and 32.2ms, respectively. Such non-monotonic behavior hereto can be attributed to the two competing mechanisms on the mixing of the fuel and oxidizer droplets prior to ignition event in the off-center collisions.

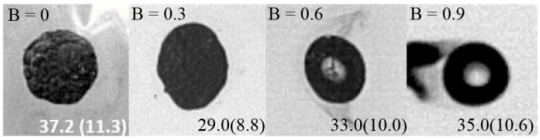

Figure 5. Nonflammable condensed-phase products from the representative cases shown in Figure 2.

Appearances of the final reaction products for the four collisions are another evidence of the non-monotonic behavior. As shown in Fig. 5, the solid-like surface appearance of the product for the cases of B = 0 and B = 0.3 implies a complete reaction, while the smooth surfaces for the cases of B = 0.6 and B = 0.9 suggest that the reduced mass transfer and hence chemical reaction result in a certain amount of unburned liquid propellant.

4. Non-monotonic Effect of Impact Parameter on Ignition Delay

The non-monotonic dependence of the ignition delay on B at We = 60.9 and Δ = 1.6 has been adequately investigated and it can be further confirmed by comparing the results at various Wes and Δs. As shown in Fig.6, the non-monotonic dependence of ignition delay on the impact parameter B can be observed. Specifically, for collisions with We = 41.0, Δ = 1.3; We = 60.9, Δ = 1.3; We = 60.9, Δ = 1.6; We = 83.0, Δ = 1.6; and We = 83.0, Δ = 2.0, the ignition delay is inversely proportional to B when B is slightly larger than 0. However, if B increases to a value about 0.3~0.4, the stretching separation happens and the time for ignition delay will be prolonged with increasing B.

Some interesting observations on the dependence of ignition delay on B can be found for large size ratios. For Δ = 2.0, the ignition delay monotonically decreases with B from 0.2 to 0.5 for We = 60.9 and from 0.4 to 0.6 for We = 41.0, as shown in Fig. 6. It will in fact turn into being non-ignitable when the collision becomes a head-on or grazing one. As reported by Zhang et al.[15], the dominant exothermic liquid-phase reaction between WFNA and TMEDA is

$$\mathrm{TMEDA} + 2\mathrm{HNO_3} \rightarrow \mathrm{TMEDADN} \qquad (2)$$

whose overall equivalence ratio for Δ = 2.0 is as low as 0.07. Consequently, the deficiency of heat release in the extremely "fuel lean" reaction and the substantial heat lost to the surrounding environment from such small droplets make the ig nitability range of B is smaller with increasing the size ratio.

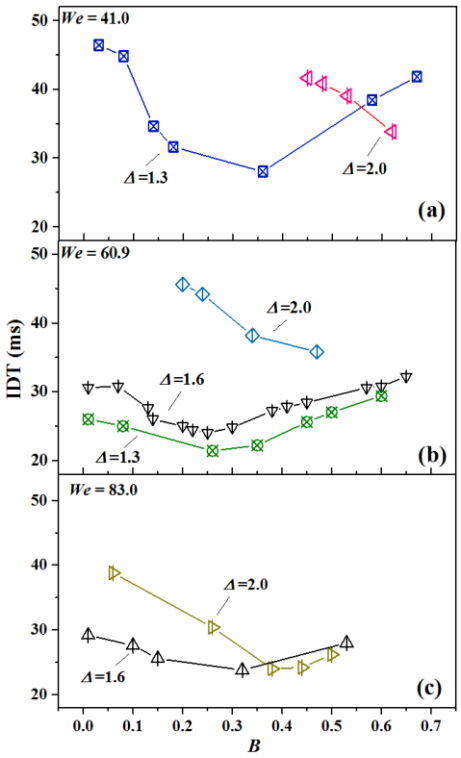

Figure 6, Dependence of ignition delay on *B* with (a)*We* = 41.0, *Δ*= 1.3 and 2.0; (2) *We* = 60.9, *Δ* = 1.3, 1.6 and 2.0; and (c) *We* = 83.0, *Δ* =1.6 and 2.0.

5 Conclusions

The hypergolic ignition induced by the binary collision by WFNA and TMEDA droplets was experimentally studied. Non-monotonic dependence of the hypergolic ignition delay on the impact parameter effect was observed and analyzed for various Weber number and size ratios. The ignition seems to be suppressed at small *Wes* and/or large size ratios. The ignitibility regime merits future study, particularly in consideration of heat lost and size effect have not been adequately studied.

6 Acknowledgment

This work was supported by the Hong Kong RGC/GRF (operating under contract numbers PolyU 152217/14E and 152651/16E) and partly by the Hong Kong Polytechnic University (G-UA2M and G-YBGA).

Reference

[1] G.P. Sutton, O. Biblarz, Rocket propulsion elements, 8ed., John Wiley & Sons, Hoboken, New Jersey, 2010.

[2] E.A. Fletcher, G. Morrell, Ignition in liquid propellant rocket engines, in: M.G. J. Ducerme, A. H. Lefebvre (Ed.), Progress in Combustion Science and Technology Volume I, Pergamon, Oxford. London. New York. Paris, 1960, pp. 183-215.

[3] R.J.M. Eric A. Hurlbert, Propellant Ignition and Flame Propagation, in: V. Yang, M. Habiballah, J. Hulka, M. Popp (Eds.), Liquid Rocket Thrust Chambers: Aspects of Modeling, Analysis, and Design, American Institute of Aeronautics and Astronautics, Inc., Virginia, 2004.

[4] M. Kilpatrick, L.L. Baker, Symp. (Int.) Combust, (1955) 196-205.

[5] S. Wang, S.T. Thynell, A, Energy & Fuels 24 (2010) 5320-5330.

[6] Forness, T.L. Pourpoint, S.D. Heister, 49th AIAA/ASME/SAE/ASEE Joint Propulsion Conference (2013) 3772.

[7] E.M. Dambach, Y. Solomon, S.D. Heister, T.L. Pourpoint, J. Propul. Power 29 (2013) 331-338.

[8] D. Zhang, P. Zhang, Y. Yuan, T. Zhang, Combust Flame 173 (2016) 276-287.

[9] C. Tang, J. Zhao, P. Zhang, C.K. Law, Z. Huang, J. Fluid Mech., 795 (2016) 671-689.

[10] C. Tang, P. Zhang, C.K. Law, Phys Fluids 24 (2012).

[11] J. Qian, C.K. Law, J. Fluid Mech. 331 (1997) 59-80.

[12] N. Ashgriz, J. Poo, J. Fluid Mech. 221 (1990) 183-204.

[13] T. Inamuro, S. Tajima, F. Ogino, International journal of heat and mass transfer 47 (2004) 4649-4657.

[14] X. Chen, D. Ma, P. Khare, V. Yang, 49th AIAA Aerospace Sciences Meeting Including the New Horizons Forum and Aerospace Exposition; 2011. p. 771.

[15] P. Zhang, L.D. Zhang, C.K. Law, Combust. Flame 162 (2015) 237-248.

[16] W.-G. Liu, S. Dasgupta, S.V. Zybin, W.A. Goddard III, The J. Phys. Chem. A 115 (2011) 5221-5229.

[17] C. Tang, J. Zhao, P. Zhang, C.K. Law, Z. Huang, J. Fluid Mech., 795 (2016) 671-689.